AEDC-TR-79-55

c.6

Analytic and Numerical Investigation of the Convergence for the Adaptive Wall Concept

C. F. Lo and W. L. Sickles
ARO, Inc.

November 1979

Final Report for Period October 1977 – March 1978

Approved for public release; distribution unlimited.

ARNOLD ENGINEERING DEVELOPMENT CENTER
ARNOLD AIR FORCE STATION, TENNESSEE
AIR FORCE SYSTEMS COMMAND
UNITED STATES AIR FORCE

NOTICES
When U. S. Government drawings, specifications, or other data are used for any purpose other than a definitely related Government procurement operation, the Government thereby incurs no responsibility nor any obligation whatsoever, and the fact that the Government may have formulated, furnished, or in any way supplied the said drawings, specifications, or other data, is not to be regarded by implication or otherwise, or in any manner licensing the holder or any other person or corporation, or conveying any rights or permission to manufacture, use, or sell any patented invention that may in any way be related thereto.
Qualified users may obtain copies of this report from the Defense Documentation Center.
References to named commerical products in this report are not to be considered in any sense as an indorsement of the product by the United States Air Force or the Government.

This report has been reviewed by the Information Office (OI) and is releasable to the National Technical Information Service (NTIS). At NTIS, it will be available to the general public, including foreign nations.

APPROVAL STATEMENT

This report has been reviewed and approved.

Alexander F. Money

ALEXANDER F. MONEY
Project Manager
Directorate of Technology

Approved for publication:

FOR THE COMMANDER

Marion L. Laster

MARION L. LASTER
Director of Technology
Deputy for Operations

REPORT DOCUMENTATION PAGE		READ INSTRUCTIONS BEFORE COMPLETING FORM
1. REPORT NUMBER AEDC-TR-79-55	2. GOVT ACCESSION NO.	3. RECIPIENT'S CATALOG NUMBER
4. TITLE (and Subtitle) ANALYTIC AND NUMERICAL INVESTIGATION OF THE CONVERGENCE FOR THE ADAPTIVE-WALL CONCEPT		5. TYPE OF REPORT & PERIOD COVERED Final Report, October 1977-March 1978 6. PERFORMING ORG. REPORT NUMBER
7. AUTHOR(s) C. F. Lo and W. L. Sickles, ARO, Inc., a Sverdrup Corporation Company		8. CONTRACT OR GRANT NUMBER(s)
9. PERFORMING ORGANIZATION NAME AND ADDRESS Arnold Engineering Development Center Air Force Systems Command Arnold Air Force Station, TN 37389		10. PROGRAM ELEMENT, PROJECT, TASK AREA & WORK UNIT NUMBERS Program Element 65807F
11. CONTROLLING OFFICE NAME AND ADDRESS Arnold Engineering Development Center/DOS Air Force Systems Command Arnold Air Force Station, TN 37389		12. REPORT DATE November 1979 13. NUMBER OF PAGES 38
14. MONITORING AGENCY NAME & ADDRESS(if different from Controlling Office)		15. SECURITY CLASS. (of this report) UNCLASSIFIED 15a. DECLASSIFICATION/DOWNGRADING SCHEDULE N/A

16. DISTRIBUTION STATEMENT (of this Report)

Approved for public release; distribution unlimited.

17. DISTRIBUTION STATEMENT (of the abstract entered in Block 20, if different from Report)

18. SUPPLEMENTARY NOTES

Available in DDC.

19. KEY WORDS (Continue on reverse side if necessary and identify by block number)

wind tunnels
walls
interference
adaptive wall concept
perturbation theory
convergence
subsonic flow

20. ABSTRACT (Continue on reverse side if necessary and identify by block number)

Convergence of the iteration for the adaptive wall concept is analytically proved for two-dimensional and axisymmetric subsonic flows. One-step convergence formulae which determine the unconfined boundary conditions directly from two measured flow variables at the measuring surface are presented to accelerate the iterative procedure. The application of the one-step formulae to numerical examples of an NACA 0012 airfoil illustrates the capability of these formulae for subcritical as well as supercritical flows.

DD FORM 1 JAN 73 1473 EDITION OF 1 NOV 65 IS OBSOLETE

PREFACE

The work reported herein was conducted by the Arnold Engineering Development Center (AEDC), Air Force Systems Command (AFSC). The results were obtained by ARO, Inc., AEDC Division (a Sverdrup Corporation Company), operating contractor for the AEDC, AFSC, Arnold Air Force Station, Tennessee, under ARO Project Numbers P32A-S3A and P32C-36. The Air Force Project Manager was Mr. Alexander F. Money, AEDC/DOT. The manuscript was submitted for publication on June 8, 1979.

CONTENTS

ILLUSTRATIONS

Figure Page

APPENDIX

1.0 INTRODUCTION

The adaptive wall concept is a systematic procedure for eliminating wall interference. Ferri and Baronti (Ref. 1) and Sears (Ref. 2) independently originated the adaptive wall concept wherein it was recognized that by measuring two flow variables and evaluating functional relationships for unconfined flow conditions, one can adjust the local wall boundary to achieve interference-free flow. The procedure is iterative, and wall boundary adjustments are made until unconfined flow is achieved at a measuring surface near the wall. The analytical investigations by Lo and Kraft (Ref. 3) and Sears (Ref. 4) have shown the feasibility of the concept. Also, a numerical simulation by Erickson and Nenni (Ref. 5) established the concept, and recent experimental studies (Refs. 6 through 9) have validated the practicality of an adaptive wall tunnel.

Since the adaptive wall procedure is iterative, the reduction of the number of wall adjustments to achieve unconfined flow would save on tunnel run time and computer time in an adaptive wall wind tunnel. This has been the impetus for the study of accelerating convergence and the development of one-step convergence formulae to evaluate the flow conditions. The one-step formulae significantly reduce the number of iterations, and under certain conditions unconfined flow can be achieved in one single step.

This report is concerned with the development of methods for use in two-dimensional and axisymmetric adaptive wall wind tunnels. Convergence of the iterative procedure and derivation of the one-step convergence formulae are presented for both two-dimensional and axisymmetric flows using linearized small disturbance theory and the Fourier transform technique.

Numerical examples of the method in which a computer program serves as an analog of the wind tunnel to simulate the interior flow field are presented. These numerical demonstrations have shown the validity of the adaptive wall procedure and the power of the one-step formulae in reducing the number of wall iterations in subsonic and transonic flows.

2.0 ITERATIVE PROCEDURE

The concept of the adaptive wall wind tunnel, as explained in Refs. 1 and 2, states that to determine whether unconfined flight conditions are obtained in a tunnel with any model, it is necessary and sufficient to match the measured flow variables at a selected control surface, say S, with the flow variables which satisfy the unconfined boundary condition. Specifically, it is necessary to measure the distributions of two independent flow variables such as the longitudinal and normal perturbation velocity components at the surface S

(which is located inside the tunnel but away from the model). One of the measured variables is used as the boundary value to uniquely specify the flow field exterior to S in the presence of the condition of unconfined, undisturbed flow of a uniform stream at infinity. Hence, since the two measured distributions constitute redundant boundary data in the presence of the exterior region far-field boundary condition, equivalence at S of the measured flow variables interior to S and the computed flow variables exterior to S constitutes a definition of interference-free flow in the wind tunnel. Therefore, by comparing the exterior region calculated values with the measured values of the same quantities, one can determine whether or not unconfined flow conditions exist.

Unconfined flow conditions can be achieved if provisions are available for adjusting the wall in a logical manner. A basic iterative procedure for adjusting the walls to achieve unconfined flow is presented in block diagram form in Fig. 1 and applies for both two- and three-dimensional flow fields. First a flow field is established in the tunnel, and the velocity components u_T and v_T are measured at the given control surface S. The exterior unconfined region is then evaluated by specifying $v_E = v_T$ as the boundary value at S. If the distribution at S of u_E determined from the exterior region calculation does not agree with u_T, then the flow is still affected by the walls and the walls must be readjusted. The iteration continues until u_E and u_T agree. Then the flow about the model in the tunnel is unconfined.

To accelerate convergence, a relaxation factor, k, is introduced in the iterative procedure as

$$u_T^{(n+1)} = k\, u_E^{(n)} + (1 - k)\, u_T^{(n)} \tag{1}$$

at S. The tunnel wall is adjusted according to Eq. (1). The proper selection for the value of k to speed up iteration convergence will be discussed later.

Alternately, $u_E = u_T$ can be specified as the boundary condition on S in the exterior region, and v_E can be compared with v_T to determine whether unconfined flow exists in the tunnel. More generally, any two independent measurable flow variables can be used in the adaptive wall procedure.

3.0 CONVERGENCE OF THE ITERATIVE PROCEDURE

To provide an analytical proof of convergence of the adaptive wall iterative procedure, an interior tunnel simulation is required in addition to an exterior flow functional relationship.

3.1 TWO-DIMENSIONAL TUNNEL

3.1.1 Exterior Flow-Field Relationships

As indicated previously, an exterior flow-field relationship is required to demonstrate the adaptive wall concept. The flow field is described by the linearized Prandtl-Glauert equation, and the boundary value problem in the exterior, unconfined flow region is shown in Fig. 2. The boundary-value problem can be solved by the Fourier transform technique using $v_E(x, \pm h)$ as the boundary value at $y = \pm h$ along with the condition of unconfined flow at infinity. The corresponding unconfined flow distribution $u_E(x, \pm h)$ at the measuring plane S is related to the $v_E(x, \pm h)$ in the transformed plane as

$$\bar{u}_E(p,\pm h) = \frac{i}{\beta}\frac{p}{|p|}\bar{v}_E(p,\pm h) \tag{2}$$

where the barred quantities are the Fourier-transformed variables defined by

$$\bar{g}(p,\pm h) = (2\pi)^{-1/2}\int_{-\infty}^{\infty} g(x,\pm h)\, e^{ipx}\, dx$$

with p being the Fourier transform parameter.

Alternately, if u_E is the boundary condition at S for the exterior region, then

$$\bar{v}_E(p,\pm h) = -i\beta\frac{p}{|p|}\bar{u}_E(p,\pm h) \tag{3}$$

Equations (2) and (3) can be inverted into the physical plane as

$$u_E(x,\pm h) = \frac{-1}{\pi\beta}\oint_{-\infty}^{\infty}\frac{v_E(\xi,\pm h)}{\xi - x}\, d\xi \tag{4}$$

and

$$v_E(x,\pm h) = \frac{\beta}{\pi}\oint_{-\infty}^{\infty}\frac{u_E(\xi,\pm h)}{\xi - x}\, d\xi \tag{5}$$

which are the familiar exterior flow functional relationships presented in Ref. 2.

3.1.2 Interior Flow-Field Simulation

Simulation of the interior flow field is required strictly for the theoretical proof of convergence. It should be emphasized that the power of the adaptive wall concept is that it never requires the calculation of the interior flow field when applied to a real wind tunnel. The measured tunnel flow is simulated here by the analytical model of the flow in the tunnel described by the boundary-value problem shown in Fig. 2.

Based on thin airfoil theory, the thickness and camber (including incidence) of an airfoil may be treated as symmetric and asymmetric problems, respectively, if the control surfaces are selected symmetrically about the airfoil. The boundary-value problem outlined in Fig. 2 can be divided into symmetrical and asymmetrical problems as given in Fig. 3. Thus, the velocity components at the control surface can also be divided into symmetrical and asymmetrical components as

$$u_T(\pm h) = u_{T_s}(\pm h) + u_{T_A}(\pm h) \tag{6}$$

and

$$v_T(\pm h) = v_{T_s}(\pm h) + v_{T_A}(\pm h) \tag{7}$$

Then the symmetric and asymmetric perturbation velocities can be written in terms of the velocity components at the control surfaces as

$$u_{T_S}(\pm h) = \frac{1}{2}\left[u_T(h) + u_T(-h)\right] \tag{8a}$$

$$v_{T_S}(\pm h) = \pm\frac{1}{2}\left[v_T(h) - v_T(-h)\right] \tag{8b}$$

$$u_{T_A}(\pm h) = \pm\frac{1}{2}\left[u_T(h) - u_T(-h)\right] \tag{9a}$$

and

$$v_{T_A}(\pm h) = \frac{1}{2}\left[v_T(h) + v_T(-h)\right] \tag{9b}$$

For the symmetric problem, the transformed normal velocity, $\bar{v}_{T_S}$, in the tunnel can be expressed as a function of the model geometry and an arbitrary distribution of the longitudinal velocity, $\bar{u}_{T_S}$, as

$$\bar{v}_{T_S}(p,h) = i\beta\frac{p}{|p|}\tanh\left(|p|\beta h\right)\bar{u}_{T_S}(p,h) + \operatorname{sech}(p\beta h)\,\bar{F}(p) \tag{10}$$

where

$$\bar{F}(p) = (2\pi)^{-1/2} \int_{-\infty}^{\infty} F_x(x)\, e^{ipx}\, dx$$

The model thickness distribution, F(x), can be interpreted as a "potential equivalent" airfoil profile including viscous effects. It is reasonable to assume that the same equivalent profile exists in an unconfined flow condition. The solution for unconfined flow is readily obtained in the transformed plane (Ref. 3) as

$$\bar{u}_{\infty_s}(p,h) = \frac{i}{\beta}\frac{p}{|p|}\, e^{-|p|\,\beta h}\, \bar{F}(p) \tag{11}$$

$$\bar{v}_{\infty_s}(p,h) = e^{-|p|\,\beta h}\, \bar{F}(p) \tag{12}$$

For the asymmetric problem, the normal velocity in the tunnel can be expressed as a function of the model camber and incidence and as an arbitrary distribution of the longitudinal velocity; thus,

$$\bar{v}_{T_A}(p,h) = i\beta\frac{p}{|p|}\coth(|p|\beta h)\,\bar{u}_{T_A}(p,h) - \frac{i\beta}{2}\frac{p}{|p|}\operatorname{csch}(|p|\beta h)\,\bar{\gamma}(p) \tag{13}$$

where

$$\bar{\gamma}(p) = (2\pi)^{-1/2} \int_{-\infty}^{\infty} \gamma(x)\, e^{ipx}\, dx$$

The distribution of vortices, $\gamma(x)$, is used to represent the model camber and incidence. With the assumption of vortex strength remaining the same for confined and unconfined flow conditions, the solution for unconfined flow is expressed as

$$\bar{u}_{\infty_A}(p,h) = \frac{1}{2}\, e^{-|p|\,\beta h}\bar{\gamma}(p) \tag{14}$$

$$\bar{v}_{\infty_A}(p,h) = \frac{i\beta}{2}\frac{p}{|p|}\, e^{-|p|\,\beta h}\,\bar{\gamma}(p) \tag{15}$$

3.1.3 Proof of Convergence

The convergence of the iteration procedure will be proved for the symmetric problem first in the transformed plane since the functional relationships and tunnel simulation are in

simple algebraic form in that plane. The iteration is initiated with an unspecified tunnel wall configuration which provides the arbitrary initial value of flow quantities, $u_{T_s}^{(o)}$ and $v_{T_s}^{(o)}$, or in the transformed plane, $\bar{u}_{T_s}^{(o)}$ and $\bar{v}_{T_s}^{(o)}$, at the measuring plane y = h. Following the iterative scheme shown in Fig. 1, one can obtain the n^{th} iterative values for $\bar{u}_{E_s}$ and $\bar{u}_{T_s}$ at y = h by appropriately utilizing Eqs. (2), (3), and (10) to yield

$$\bar{u}_{E_s}^{(n)}(p,h) = \begin{cases} -\frac{p}{|p|}\tanh(p\beta h)\,\bar{u}_{T_s}^{(o)}(p,h) + \frac{i}{\beta}\Lambda, n = 0 \\ -\frac{p}{|p|}\tanh(p\beta h)\,G^{(n)} + \frac{i}{\beta}\Lambda, \\ n = 1, 2, \ldots \end{cases} \tag{16}$$

and

$$\bar{u}_{T_s}^{(n)}(p,h) = \omega\,\bar{u}_{E_s}^{(n-1)}(p,h) + (1-\omega)\,\bar{u}_{T_s}^{(n-1)}(p,h) = G^{(n)}, n = 1, 2, \ldots \tag{17}$$

where ω is a relaxation factor defined in the transformed plane to accelerate convergence and

$$G^{(n)} = \Omega^{n-1}\,G^{(1)} + \frac{i\omega}{\beta}\,\frac{(1-\Omega^{n-1})}{(1-\Omega)}\,\Lambda, n = 2, 3, \ldots \tag{18}$$

where

$$G^{(1)} = \frac{i\omega}{\beta}\,\frac{p}{|p|}\,\bar{v}_{T_s}^{(o)}(p,h) + (1-\omega)\,\bar{u}_{T_s}^{(o)}(p,h) \tag{19}$$

$$\Omega = 1 - \omega\left[1 + \tanh\left(|p|\beta h\right)\right] \tag{20}$$

$$\Lambda = \frac{p}{|p|}\,\mathrm{sech}(p\beta h)\,\bar{F}(p) \tag{21}$$

It should be noted that $\Omega^2 < 1$ for $0 < \omega < 1$. As the iteration proceeds, the effect of the initial tunnel conditions (represented by $G^{(1)}$) diminishes. In the limit as $n \to \infty$ it is readily established that

$$\lim_{n\to\infty} G^{(n)} = \frac{i\omega\Lambda}{\beta(1-\Omega)} = \frac{i}{\beta}\,\frac{p}{|p|}\,e^{-|p|\beta h}\,\bar{F}(p) \tag{22}$$

which is equal to $\bar{u}_\infty(p,h)$ as indicated in Eq. (11). Consequently, in the limit $n \to \infty$

$$\lim_{n \to \infty} \bar{u}_{E_s}^{(n)}(p,h) = \lim_{n \to \infty} \bar{u}_{T_s}^{(n)}(p,h) = \lim_{n \to \infty} G^{(n)} = \bar{u}_{\infty_s}(p,h) \tag{23}$$

and, hence, convergence of the adaptive wall method to unconfined flow is established independent of the initial tunnel conditions for nonlifting airfoils in subsonic flow. It is important to note that the iteration procedure converges independently of the relaxation factor for values $0 < \omega < 1$. It should also be noted that convergence can be demonstrated in a similar manner for the alternate procedure of specifiying v_{T_s} instead of u_{T_s} at the control surface.

Similarly, the asymmetric problem can be shown by using Eqs. (2), (3), and (13) following the scheme shown in Fig. 1. Since the problem is linear, the general problem including the symmetric and asymmetric portion is also convergent independent of the initial tunnel conditions.

3.2 AXISYMMETRIC TUNNEL

3.2.1 Exterior Flow-Field Relationships

The flow field in the region exterior to and including a circular measuring surface at $r = R$ is described by the linear potential flow equation in axisymmetric coordinates and is shown in Fig. 4. With the boundary condition specified at $r = R$ as $v_E(x,R)$ and at infinity as unconfined flow, the potential flow equation can be solved by Fourier transforms for the exterior region. The corresponding flow distribution, $u_E(x,R)$, at the measuring surface ($r = R$) is related to $v_E(x,R)$ in the transformed plane by

$$\bar{u}_E(p,R) = \frac{i}{\beta} \frac{p}{|p|} \frac{K_o(|p|\beta R)}{K_1(|p|\beta R)} \bar{v}_E(p,R) \tag{24}$$

where K_o and K_1 are modified Bessel functions of zero and first order.

If u_E is specified as the boundary condition at $r = R$, then

$$\bar{v}_E(p,R) = -i\beta \frac{p}{|p|} \frac{K_1(|p|\beta R)}{K_o(|p|\beta R)} \bar{u}_E(p,R) \tag{25}$$

The unconfined flow field is determined about a body of revolution with its axis at r = 0. Using the Fourier transform technique, one can derive the streamwise and normal velocity components at the measuring surface as

$$\bar{u}_\infty (p,R) = ip\, K_o(|p|\beta R)\, \bar{Q}(p) \tag{26}$$

and

$$\bar{v}_\infty (p,R) = |p|\, K_1(|p|\beta R)\, \bar{Q}(p) \tag{27}$$

where

$$Q(p) = (2\pi)^{-1/2} \int_{-\infty}^{\infty} Q_x (x)\, e^{ipx}\, dx$$

3.2.2 Interior Flow-Field Simulation

In order to verify convergence of the iterative procedure, it is necessary to mathematically simulate the interior flow field as shown in Fig. 4. If the linear potential flow equation in the transformed plane is used with boundary conditions specified as $\bar{v}_T(p,R)$ and the model geometry as used in Eq. (26), the solution to the boundary-value problem for the interior region can be derived as

$$\bar{u}_T(p,R) = \frac{i}{\beta}\frac{p}{|p|}\frac{I_o(|p|\beta R)}{I_1(|p|\beta R)}\bar{v}_T(p,R) + \frac{i}{\beta}\frac{p}{|p|}\frac{\bar{Q}(p)}{R\, I_1(|p|\beta R)} \tag{28}$$

where I_o and I_1 are modified Bessel functions. If $\bar{u}_T(p,R)$ is specified, the solution becomes

$$\bar{v}_T(p,R) = i\beta\frac{p}{|p|}\frac{I_1(|p|\beta R)}{I_o(|p|\beta R)}\bar{u}_T(p,R) + \frac{\bar{Q}(p)}{R\, I_o(|p|\beta R)} \tag{29}$$

3.2.3 Proof of Convergence

In the transformed plane, convergence of the iterative procedure shown in Fig. 1 can be demonstrated. Using Eqs. (24), (25), (28), and (29), the n^{th} iterative values of $\bar{u}_E(p,R)$ and $\bar{u}_T(p,R)$ are determined from given initial values, $u_T^{(o)}(p,R)$ and $v_T^{(o)}(p,R)$, to be

$$\bar{u}_E^{(n)}(p,R) = \begin{cases} -\dfrac{K_o(|p|\beta R)\, I_1(|p|\beta R)}{K_1(|p|\beta R)\, I_o(|p|\beta R)}\ \bar{u}_T^{(o)}(p,R) + \dfrac{i}{\beta}\ \Lambda, \quad n = 0 \\ -\dfrac{K_o(|p|\beta R)\, I_1(|p|\beta R)}{K_1(|p|\beta R)\, I_o(|p|\beta R)}\ G^{(n)} + \dfrac{i}{\beta}\ \Lambda, \\ n = 1, 2, \ldots \end{cases} \tag{30}$$

and

$$\bar{u}_T^{(n)}(p,R) = \omega\, \bar{u}_E^{(n-1)}(p,R) + (1-\omega)\, \bar{u}_T^{(n-1)}(p,R)$$

$$= G^{(n)}, \quad n = 1, 2, \ldots \tag{31}$$

where ω is a relaxation factor defined in the transformed plane and is selected to accelerate convergence. The recurrence relationship of the iterative scheme is

$$G^{(n)} = \Omega^{n-1} G^{(1)} + i\ \frac{\omega}{\beta}\ \frac{1-\Omega^{n-1}}{1-\Omega}\ \Lambda, \quad n = 2, 3, \ldots \tag{32}$$

where

$$G^{(1)} = i\,\frac{\omega}{\beta}\ \bar{v}_T^{(o)}(p,R) + (1-\omega)\ \bar{u}_T^{(o)}(p,R) \tag{33}$$

$$\Omega = 1 - \omega\left[1 + \frac{K_o(|p|\beta R)\, I_1(|p|\beta R)}{K_1(|p|\beta R)\, I_o(|p|\beta R)}\right] \tag{34}$$

$$\Lambda = \frac{1}{R}\ \frac{K_o(|p|\beta R)\, \bar{Q}(p)}{I_o(|p|\beta R)\, K_1(|p|\beta R)} \tag{35}$$

It can be shown that $\Omega^2 < 1$ for $0 < \omega < 1$. With this restriction on ω, the effects of the initial conditions diminish as the iteration proceeds. In the limit as $n \to \infty$, the recurrence relationship becomes

$$\lim_{n \to \infty} G^{(n)} = i\,\frac{\omega\Lambda}{\beta}\ \frac{1}{1-\Omega} = ip\, K_o(|p|\beta R)\, \bar{Q}(p)$$

which is equal to $\bar{u}_\infty(p,R)$ as indicated in Eq. (26). Also, in the limit as $n \to \infty$,

$$\lim_{n\to\infty} \bar{u}_E^{(n)}(p,R) = \lim_{n\to\infty} \bar{u}_T^{(n)}(p,R) = \lim_{n\to\infty} G^{(n)} = \bar{u}_\infty(p,R)$$

and, hence, convergence for the axisymmetric iterative scheme has been established which is independent of the initial conditions.

4.0 ONE-STEP CONVERGENCE FORMULAE

A technique to speed up the convergence of the iteration process is important, as indicated before. For subsonic flow, a formula can be derived for determining conditions of unconfined flow in one single step. Consequently, for an adaptive wall wind tunnel it is conceivable that unconfined flow could be attained in a single adjustment of the tunnel boundary.

4.1 TWO-DIMENSIONAL TUNNEL

The conditions for unconfined flow in a tunnel can be achieved by properly choosing an optimal relaxation factor. From Eq. (20), the optimal relaxation factor, ω, can be obtained by setting $\Omega = 0$ as

$$\omega_{opt} = \frac{1}{1 + \tanh(|p|\beta h)} \tag{36}$$

which is in the transformed plane. One-step convergence formulae are derived by substituting ω_{opt} of Eq. (36) into Eq. (17) as given in Ref. 3 for the symmetric case.

Alternately, one can obtain one-step formulae to relate the unconfined flow variables with tunnel variables through the model profiles. Specifically, the elimination of $\bar{F}(p)$ between Eqs. (10), (11), and (12) yields the one-step formulae for the symmetric problem as

$$\bar{u}_{\infty_s}(p,h) = e^{-|p|\beta h}\left[\sinh(|p|\beta h)\,\bar{u}_{T_s}(p,h) + \frac{i}{\beta}\,\frac{p}{|p|}\,\cosh(p\beta h)\,\bar{v}_{T_s}(p,h)\right] \tag{37}$$

and

$$\bar{v}_{\infty_s}(p,h) = -e^{|p|\beta h}\left[i\beta\frac{p}{|p|}\,\sinh(|p|\beta h)\,\bar{u}_{T_s}(p,h) - \cosh(p\beta h)\,\bar{v}_{T_s}(p,h)\right] \tag{38}$$

Similarly, one combines Eqs. (13), (14), and (15) to eliminate the distribution of vortices, $\bar{\gamma}(p)$, and obtains the one-step formulae directly related to the tunnel flow variables, $\bar{u}_{T_A}$ and $\bar{v}_{T_A}$, at the upper control surfaces as

$$\bar{u}_{\infty_A}(p,h) = e^{-|p|\beta h}\left[\cosh(p\beta h)\,\bar{u}_{T_A}(p,h) + \frac{i}{\beta}\frac{p}{|p|}\sinh(|p|\beta h)\,\bar{v}_{T_A}(p,h)\right] \tag{39}$$

and

$$\bar{v}_{\infty_A}(p,h) = -e^{-|p|\beta h}\left[i\beta\frac{p}{|p|}\cosh(p\beta h)\,\bar{u}_{T_A}(p,h) - \sinh(|p|\beta h)\,\bar{v}_{T_A}(p,h)\right] \tag{40}$$

For a thin airfoil, the desired one-step formulae are obtained by superposition of thickness and camber effects from Eqs. (37), (38), (39), and (40) with the aid of Eqs. (8) and (9).

$$\begin{aligned}\bar{u}_\infty(h) &= \bar{u}_{\infty_s}(h) + \bar{u}_{\infty_A}(h)\\ &= \frac{1}{2}e^{-|p|\beta h}\left[e^{|p|\beta h}\bar{u}_T(h) - e^{-|p|\beta h}\bar{u}_T(-h)\right.\\ &\quad\left. + \frac{i}{\beta}\frac{p}{|p|}e^{|p|\beta h}\bar{v}_T(h) - \frac{i}{\beta}\frac{p}{|p|}e^{-|p|\beta h}\bar{v}_T(-h)\right]\end{aligned} \tag{41}$$

$$\begin{aligned}\bar{v}_\infty(h) &= -\frac{1}{2}e^{|p|\beta h}\left[-e^{-|p|\beta h}\bar{v}_T(h) + e^{|p|\beta h}\bar{v}_T(-h)\right.\\ &\quad\left. + i\beta\frac{p}{|p|}e^{|p|\beta h}\bar{u}_T(h) - i\beta\frac{p}{|p|}e^{-|p|\beta h}\bar{u}_T(-h)\right]\end{aligned} \tag{42}$$

Similarly, $\bar{u}_\infty(-h)$, $\bar{v}_\infty(h)$ at the lower control surface can also be obtained. The above pair of equations can be inverted into the physical plane as the following expressions:

$$\begin{aligned}u_\infty(x,\pm h) &= \frac{1}{2}u_T(x,\pm h) - \frac{\beta h}{\pi}\int_{-\infty}^{\infty}\frac{u_T(\xi,\mp h)}{k(\xi-x)}\,d\xi\\ &\quad \mp\frac{1}{2\pi\beta}\oint_{-\infty}^{\infty}\frac{v_T(\xi,\pm h)}{\xi-x}\,d\xi \pm \frac{1}{2\pi\beta}\int_{-\infty}^{\infty}\frac{v_T(\xi,\mp h)}{k(\xi-x)}(\xi-x)\,d\xi\end{aligned} \tag{43}$$

and

$$v_\infty(x,\pm h) = \frac{1}{2} v_T(x,\pm h) - \frac{\beta h}{\pi} \int_{-\infty}^{\infty} \frac{v_T(\xi,\mp h)}{k(\xi-x)}\, d\xi$$

$$\pm \frac{\beta}{2\pi} \oint_{-\infty}^{\infty} \frac{u_T(\xi,\pm h)}{\xi-x}\, d\xi \mp \frac{\beta}{2\pi} \int_{-\infty}^{\infty} \frac{u_T(\xi,\mp h)}{k(\xi-x)}\,(\xi-x)\, d\xi \tag{44}$$

where

$$k(\xi-x) = (2\beta h)^2 + (\xi-x)^2$$

and u_∞, u_T, v_∞, and v_T are the perturbation flow variables. The preceding one-step convergence formulae give the unconfined flow variables, $u_\infty(x,\pm h)$ and $v_\infty(x,\pm h)$ at the control surface, when the flow variables, $u_T(x,\pm h)$ and $v_T(x,\pm h)$, are in hand for any arbitrary model.

4.2 AXISYMMETRIC TUNNEL

As in the two-dimensional case, the one-step formulae for accelerating convergence can be derived by relating tunnel variables in Eqs. (28) and (29) with the unconfined variables in Eqs. (26) and (27) and eliminating the model geometry $\bar{Q}(p)$ to obtain

$$\bar{u}_\infty(p,R) = ip\beta R\, k_o(|p|\beta R)\left[\frac{I_o(|p|\beta R)}{\beta}\,\bar{v}_T(p,R) - i\frac{p}{|p|}\, I_1(|p|\beta R)\,\bar{u}_T(p,R)\right] \tag{45}$$

and

$$\bar{v}_\infty(p,R) = |p|\beta R\, k_1(|p|\beta R)\left[I_o(|p|\beta R)\,\bar{v}_T(p,R) - i\beta\frac{p}{|p|} I_1(|p|\beta R)\,\bar{u}_T(p,R)\right] \tag{46}$$

An approximate expression in the physical plane is derived for Eq. (45) in Appendix A. The resulting expression is

$$u_\infty(x,R) = \frac{1}{2}\left[u_T(x,R) + u_E(x,R)\right]$$

$$-\frac{1}{\pi\beta} \sum_{m=1}^{M} b_m \int_{-\infty}^{\infty} \frac{v_T(\xi,R)\cdot(\xi-x)}{(\xi-x)^2 + (m\beta R/2)^2}\, d\xi$$

$$-\frac{1}{\pi} \sum_{m=1}^{M} c_m \int_{-\infty}^{\infty} \frac{u_T(\xi,R)\cdot(m\beta R/2)}{(\xi-x)^2 + (m\beta R/2)^2}\, d\xi \tag{47}$$

where u_E is the exterior flow functional relationship equation, Eq. (24),

$$u_E(x,R) = -\frac{1}{\pi\beta}\int_{-\infty}^{\infty}\frac{v_T(\xi,R)}{\xi-x}\,d\xi - \frac{1}{\pi\beta}\sum_{m=1}^{M} a_m \int_{-\infty}^{\infty}\frac{v_T(\xi,R)\cdot(\xi-x)}{(\xi-x)^2+(m\beta R/2)^2}\,d\xi$$

where a_m, b_m, and c_m are coefficients of exponential curve fits to Bessel functions defined in Appendix A.

An expression for the other unconfined variables $v_\infty(x,R)$ has not been inverted into the physical plane. In the following numerical examples, this variable is not required directly but can be determined from the finite-difference computation on the next iteration using $u_\infty(x,R)$ as the boundary condition for the interior flow field.

5.0 NUMERICAL EXAMPLES

5.1 TWO-DIMENSIONAL TUNNEL

5.1.1 Subcritical Flow

An NACA 0012 airfoil at zero angle of attack and M = 0.6 is chosen as the first example to illustrate the convergence of the adaptive wall iterative procedure. For simplicity, the open-jet boundary is selected at the control surface symmetrically; i.e., $u_T^{(o)}(x,\pm h) = 0$. The interior flow field is computed by the transonic airfoil program TSFOIL (Ref. 10) to obtain $v_T^{(o)}(x,\pm h)$ as shown in Fig. 5 by a dashed line. Notice that the normal perturbation velocity component is converted to degrees to make it consistent with units of flow angle.

With the distributions of $u_T^{(o)}(x,\pm h)$, $v_T^{(o)}(x,\pm h)$, the basic iterative procedure outlined in Fig. 1 is carried out using Eq. (1) with k = 1.0. The boundary condition is updated on each successive iteration by the exterior relationship in Eq. (4) and convergence to the unconfined distributions is achieved by the fifth iteration. The results for the velocity components at the control surface are presented in Fig. 5 and for the airfoil surface pressure distribution in Fig. 6.

Using one-step formulae, Eqs. (43) and (44), with the same initial distributions of $u_T^{(o)}(x,\pm h)$ and $v_T^{(o)}(x,\pm h)$, one can determine the $u_\infty(x,\pm h)$ and $v_\infty(x,\pm h)$ at the control surface in a single step. These distributions are in good agreement with a separate computation with TSFOIL for unconfined flow as shown in Fig. 7, which demonstrates the capability of the one-step formulae. Furthermore, with the boundary conditions specified as $u_\infty(\pm h)$ or $v_\infty(\pm h)$ in the tunnel region, the airfoil surface pressure distribution is obtained as shown in Fig. 8, which shows excellent agreement with the unconfined solution.

The second example is a lifting case with a NACA 0012 airfoil at $\alpha = 1$ deg and $M = 0.6$. Starting from a closed tunnel, i.e., $v_T^{(o)}(x, \pm h) = 0$ at the control surface, the distribution of $u_T^{(o)}(x, \pm h)$ using TSFOIL is presented in Fig. 9. With the distribution of $u_T^{(o)}(x, \pm h)$, $v_T^{(o)}(x, \pm h)$, the one-step equation determines $u_\infty(x, \pm h)$, $v_\infty(x, \pm h)$ which agrees with a separate TSFOIL computation as shown in Fig. 9. Similarly, the airfoil pressure distribution illustrates the excellent agreement with unconfined flow results as shown in Fig. 10.

5.1.2 Supercritical Flow

For subsonic Mach numbers with locally supercritical flow, the one-step formulae can be used in the iteration procedure to accelerate convergence. An NACA 0012 airfoil at $M = 0.8$, $\alpha = 0$ yields results as shown in Fig. 11 with only one additional iteration to achieve convergence. For lifting conditions $M = 0.72$ and $\alpha = 1$ deg, convergence is also achieved by the second iteration as shown in Fig. 12.

5.2 AXISYMMETRIC TUNNEL

Two numerical examples chosen to demonstrate convergence of the iterative procedure for axisymmetric flow have utilized the one-step expression of Eq. (47). In both examples a transonic small disturbance program is used to simulate the interior tunnel flow field over a parabolic arc body of revolution with fineness ratio of ten. The boundary condition, $u_T(R)$ at the control surface, is varied on each successive iteration based on the calculations from Eq. (47). In the first example, the flow is subcritical throughout, and in the second example the flow field is supercritical in the vicinity of the model but subcritical at the control surface.

In the first example, Mach number is 0.9, R/ℓ is 0.5, and the initial condition, $u_T^{(o)}(x,R)$, represents an open jet boundary condition. The flow field is subcritical and remains subcritical when the boundary conditions are updated from Eq. (47). Therefore, convergence to the unconfined flow conditions using the one-step formula should be achieved on the first iteration. The results in Fig. 13 verify that convergence has been reached on the first iteration for the control surface velocity component distributions and the body surface pressure distribution.

In the second example, Mach number is 0.975, R/ℓ is 1.0, and the initial condition, $u_T(x,R)$, is selected as an open jet boundary condition. Because of the increased Mach number, the flow field becomes supercritical but remains subcritical at the control surface. Under these conditions, the one-step convergence formulae accelerate convergence. Convergence is achieved on the third iteration as indicated in Fig. 14.

6.0 CONCLUDING REMARKS

The analytic proof of convergence of the adaptive wall method using the subsonic small perturbation theory has established the validity of the concept of the adaptive wall wind tunnel. The development of one-step convergence formulae to increase the convergence speed of the iterative procedure has provided the practicality of the adaptive wall method. Numerical simulations have demonstrated the effectiveness of one-step formulae in accelerating convergence for both subsonic and transonic flows.

REFERENCES

1. Ferri, A. and Baronti, P. "A Method for Transonic Wind-Tunnel Corrections." *AIAA Journal*, Vol. 11, No. 1, January 1973, pp. 63-66.

2. Sears, W. R. "Self Correcting Wind Tunnels." Calspan Report No. RK5070-A-2, July 1973; also *The Aeronautical Journal*, Vol. 78, No. 758/759, February/March 1974, pp. 80-89.

3. Lo, C. F. and Kraft, E. M. "Convergence of the Adaptive-Wall Wind Tunnel." *AIAA Journal*, Vol. 16, No. 1, January 1978, pp. 67-72.

4. Sears, W. R. "A Note on Adaptive-Wall Wind Tunnels." AZMP 28, 1977, pp. 915-927.

5. Erickson, J. C., Jr. and Nenni, J. P. "A Numerical Demonstration of the Establishment of Unconfined-Flow Conditions in a Self-Correcting Wind Tunnel." Calspan Report RK-5070-A-1, November 1973.

6. Vidal, R. J., Erickson, J. C., Jr., and Catlin, P. A. "Experiments with a Self-Correcting Wind Tunnel." Paper No. 11, AGARD Conference Proceedings No. 174 on Wind Tunnel Design and Testing Techniques, October 1975.

7. Chevallier, J. P. "Soufflerie Transsonique a Parois Auto-Adaptables." Paper No. 12, AGARD Conference Proceedings No. 174 on Wind Tunnel Design and Testing Techniques, October 1975.

8. Goodyer, M. J. "A Low Speed Self-Streamlining Wind Tunnel." Paper No. 13, AGARD Conference Proceedings No. 174 on Wind Tunnel Design and Testing Techniques, October 1975.

9. Kraft, E. M. and Parker, R. L. "Experiments with the Reduction of Wind Tunnel Boundary Interference by the Adaptive Wall Technology." AEDC-TR-79-51, October 1979.

10. Murman, E. M., Bailey, F. R., and Johnson, M. L. "TSFOIL - A Computer Code for Two-Dimensional Transonic Calculations, Including Wind-Tunnel Wall Effects and Wave-Drag Evaluation." NASA SP-347, March 1975, pp. 769-788.

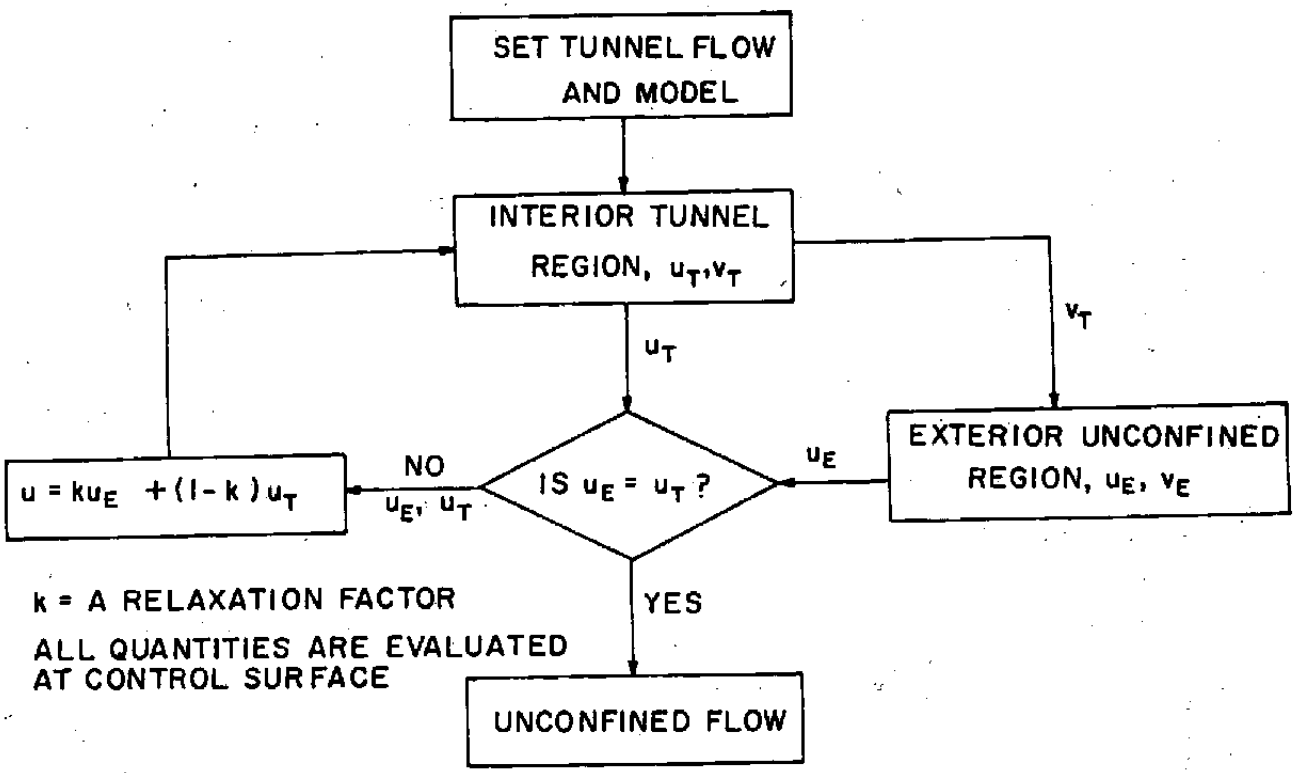

Figure 1. Block diagram of the iterative procedure of the adaptive wall concept.

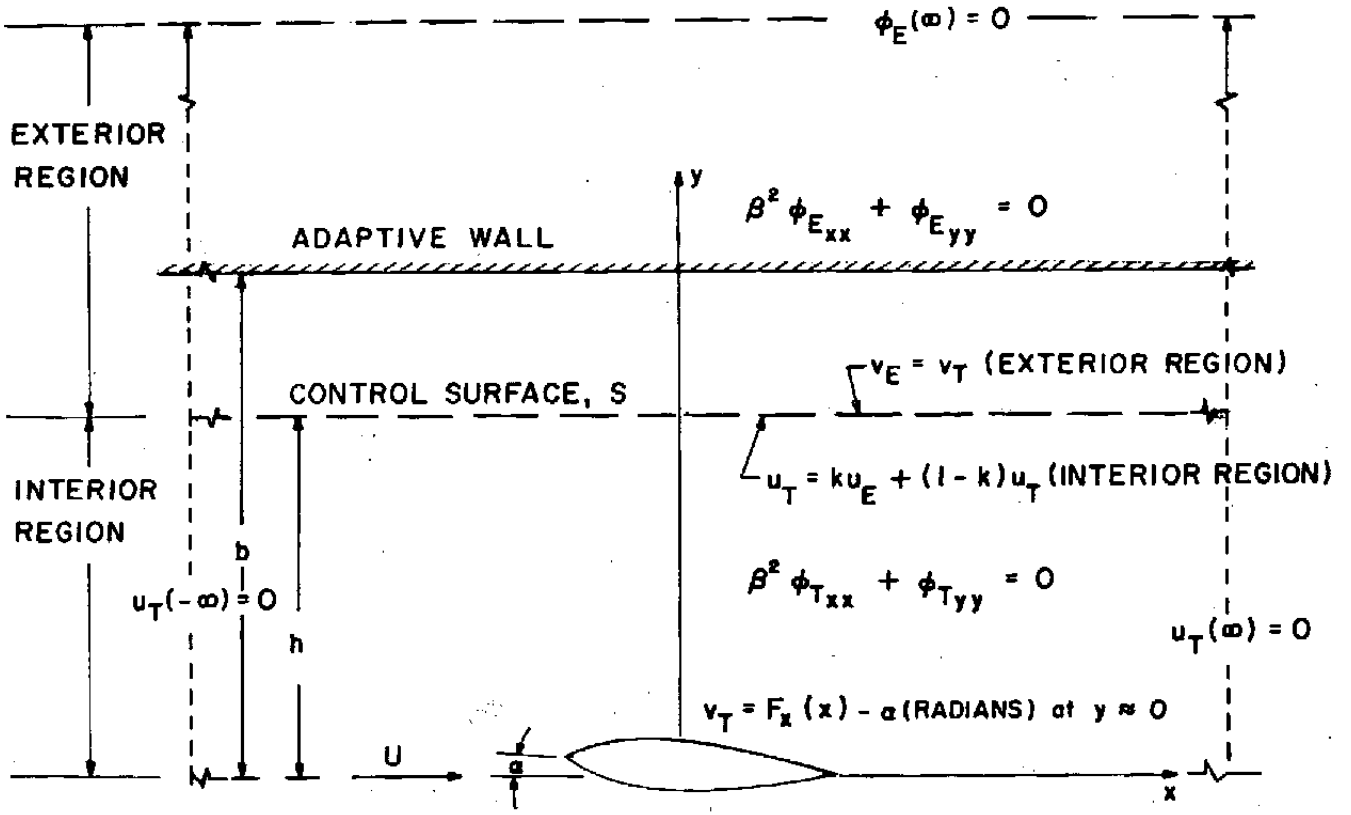

Figure 2. Two-dimensional boundary-value problem of exterior unconfined region and interior tunnel region.

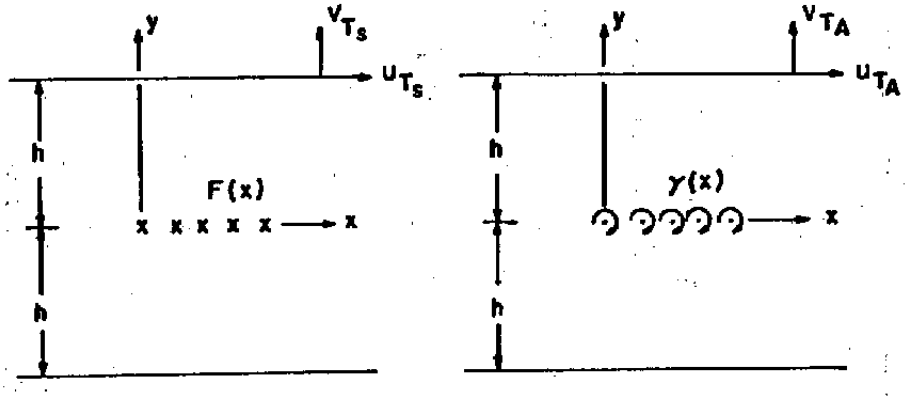

$u_{T_S}(h) = u_{T_S}(-h)$

$v_{T_S}(h) = -v_{T_S}(-h)$

a. Thickness problem

$u_{T_A}(h) = -u_{T_A}(-h)$

$v_{T_A}(h) = v_{T_A}(-h)$

b. Lifting problem

Figure 3. Mathematical model for thickness and lifting problems.

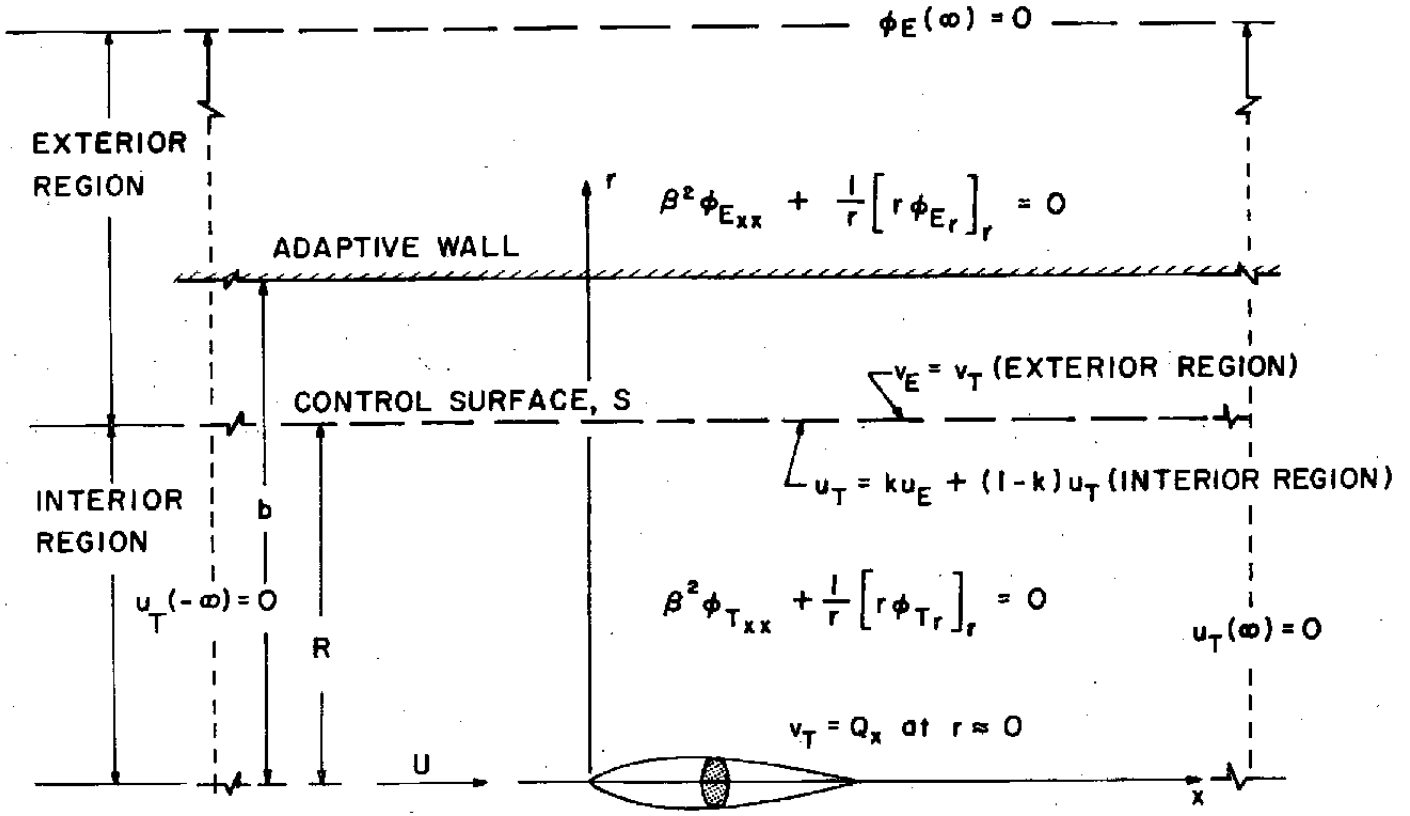

Figure 4. Axisymmetric boundary-value problem of exterior unconfined region and interior tunnel region.

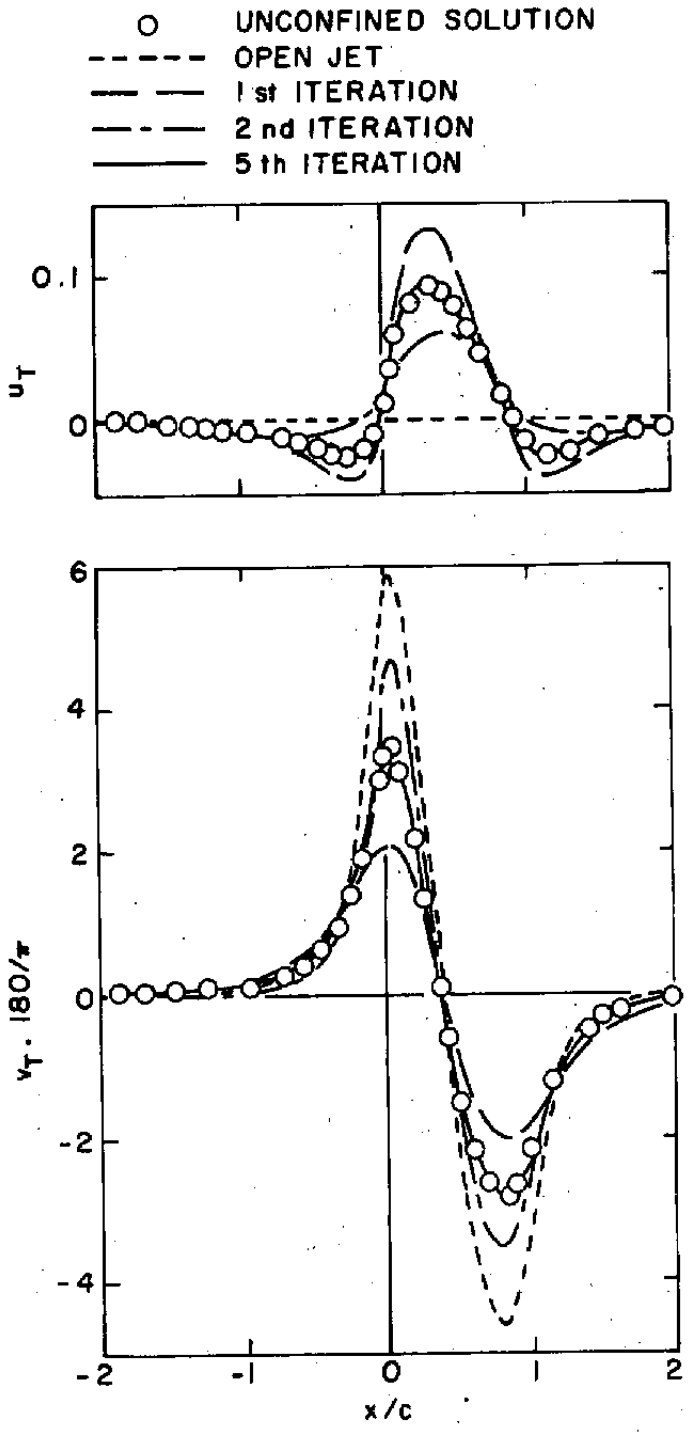

Figure 5. Velocity component distributions from iterative procedure for NACA 0012 airfoil, k = 1.0 at the control surface, h/c = 0.3, M = 0.6, α = 0.

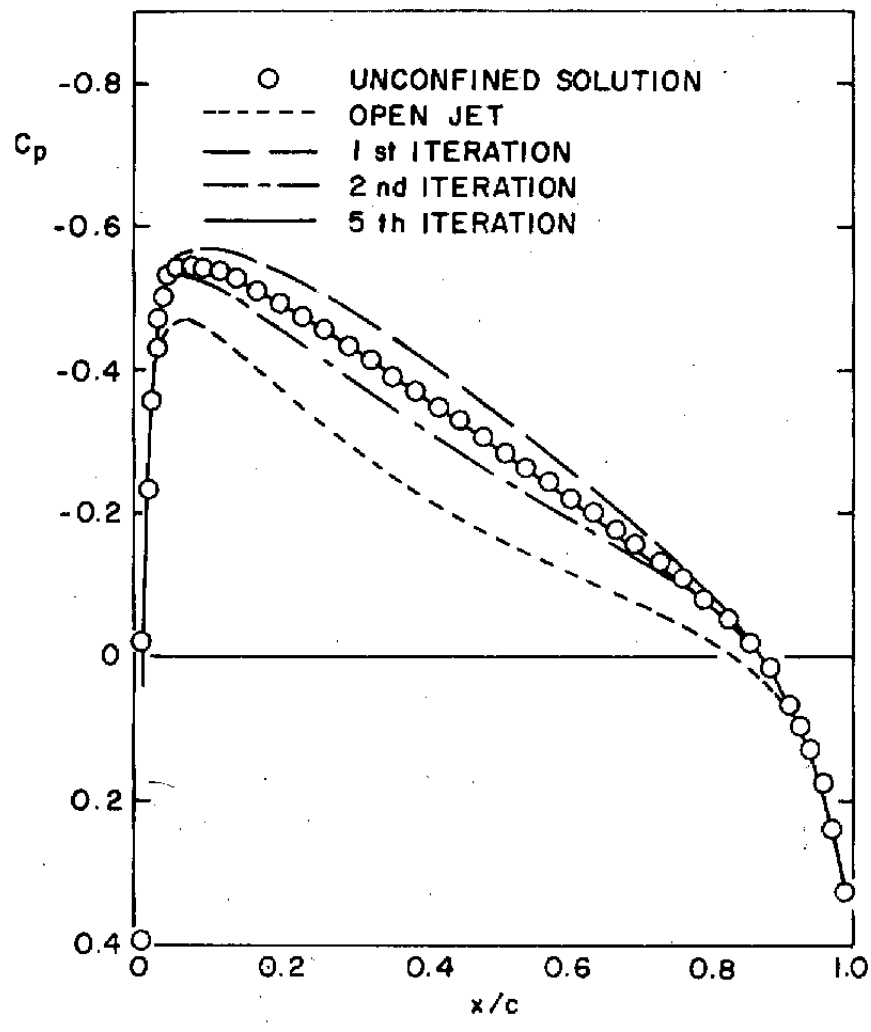

Figure 6. Airfoil surface pressure distributions based on iterative procedure results for NACA 0012 airfoil, h/c = 0.3, M = 0.6, α = 0.

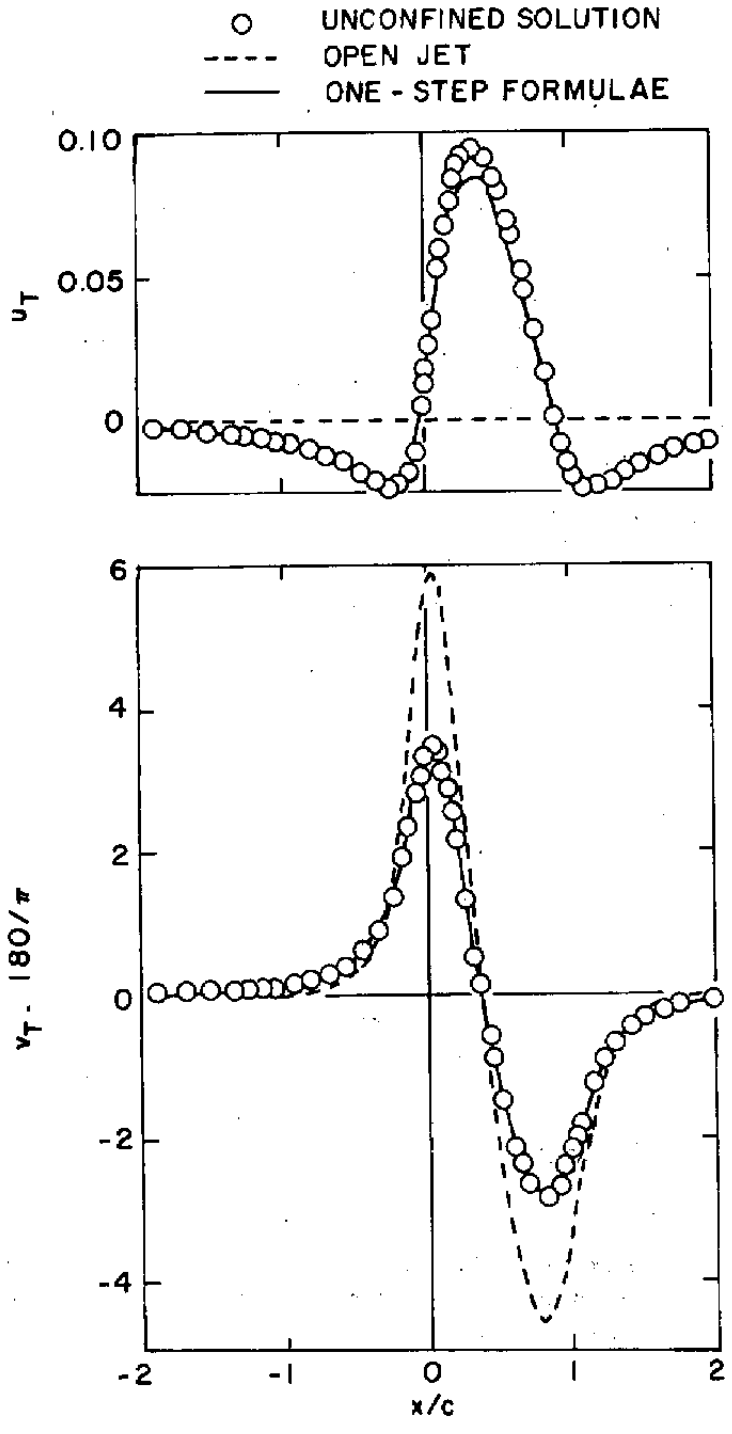

Figure 7. Velocity component distributions from one-step formulae at the control surface for NACA airfoil, h/c = 0.3, M = 0.6, α = 0.

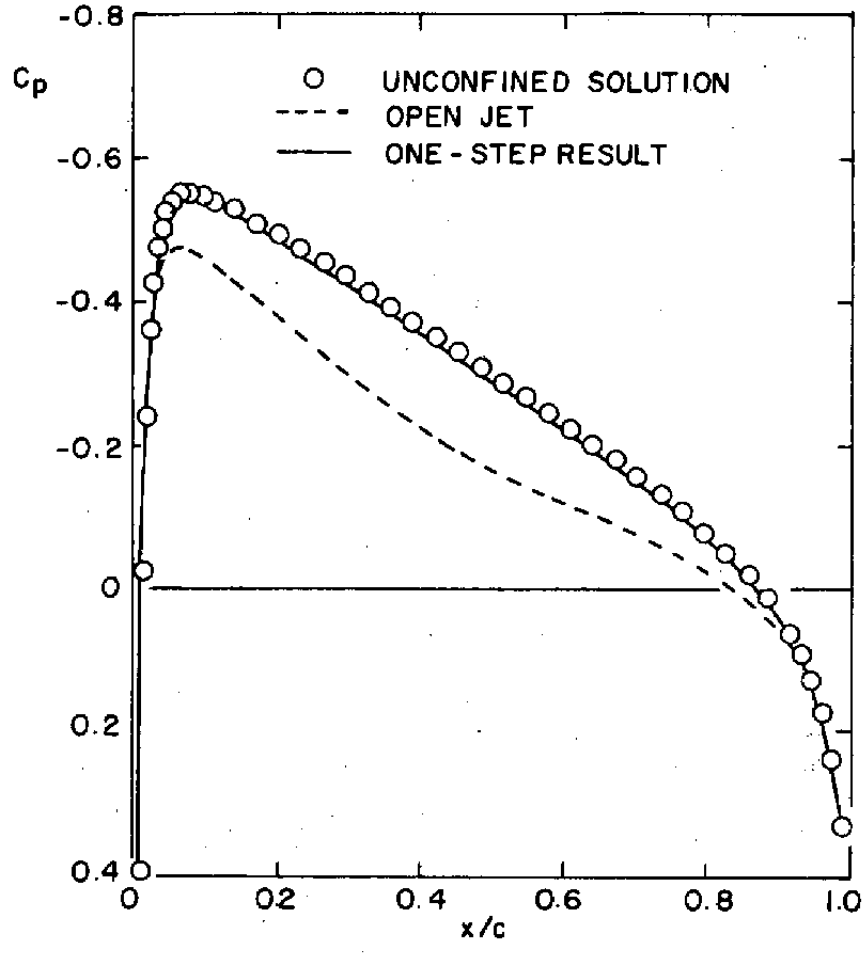

Figure 8. Airfoil surface pressure distributions based on one-step results for NACA 0012 airfoil, h/c = 0.3, M = 0.6, α = 0.

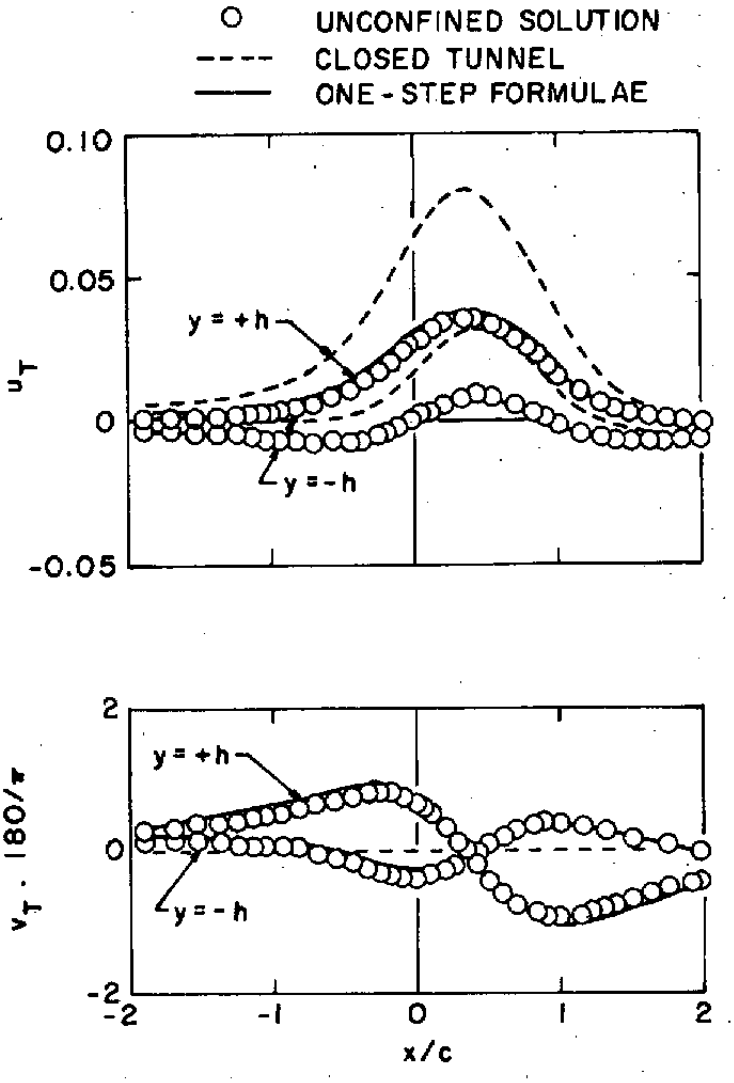

Figure 9. Velocity component distributions from one-step formulae at the control surface for NACA 0012 airfoil, h/c = 1.0, M = 0.6, α = 1.0.

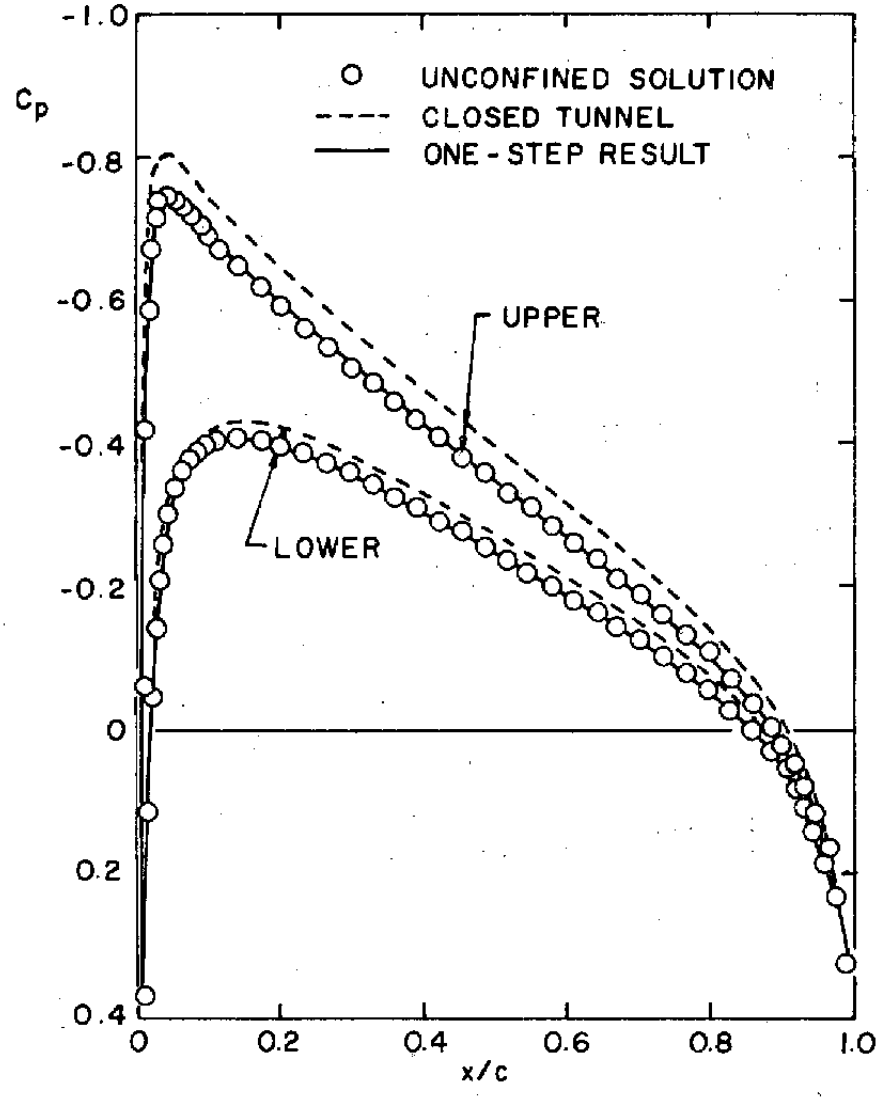

Figure 10. Airfoil surface pressure distributions based on one-step results for NACA 0012 airfoil, h/c = 1.0, M = 0.6, α = 1.0.

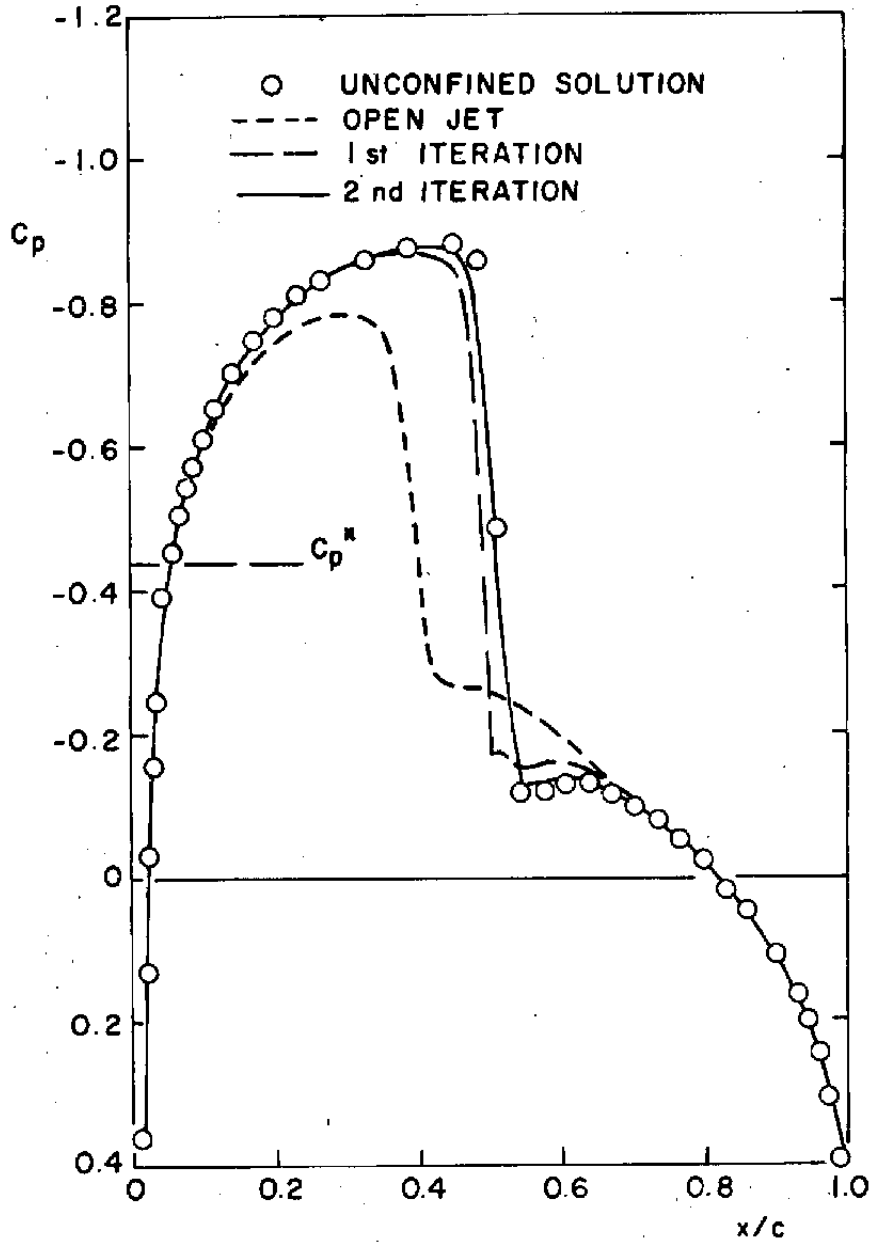

Figure 11. Airfoil surface pressure distributions based on one-step results for NACA 0012 airfoil, h/c = 1.0, M = 0.8, a = 0.

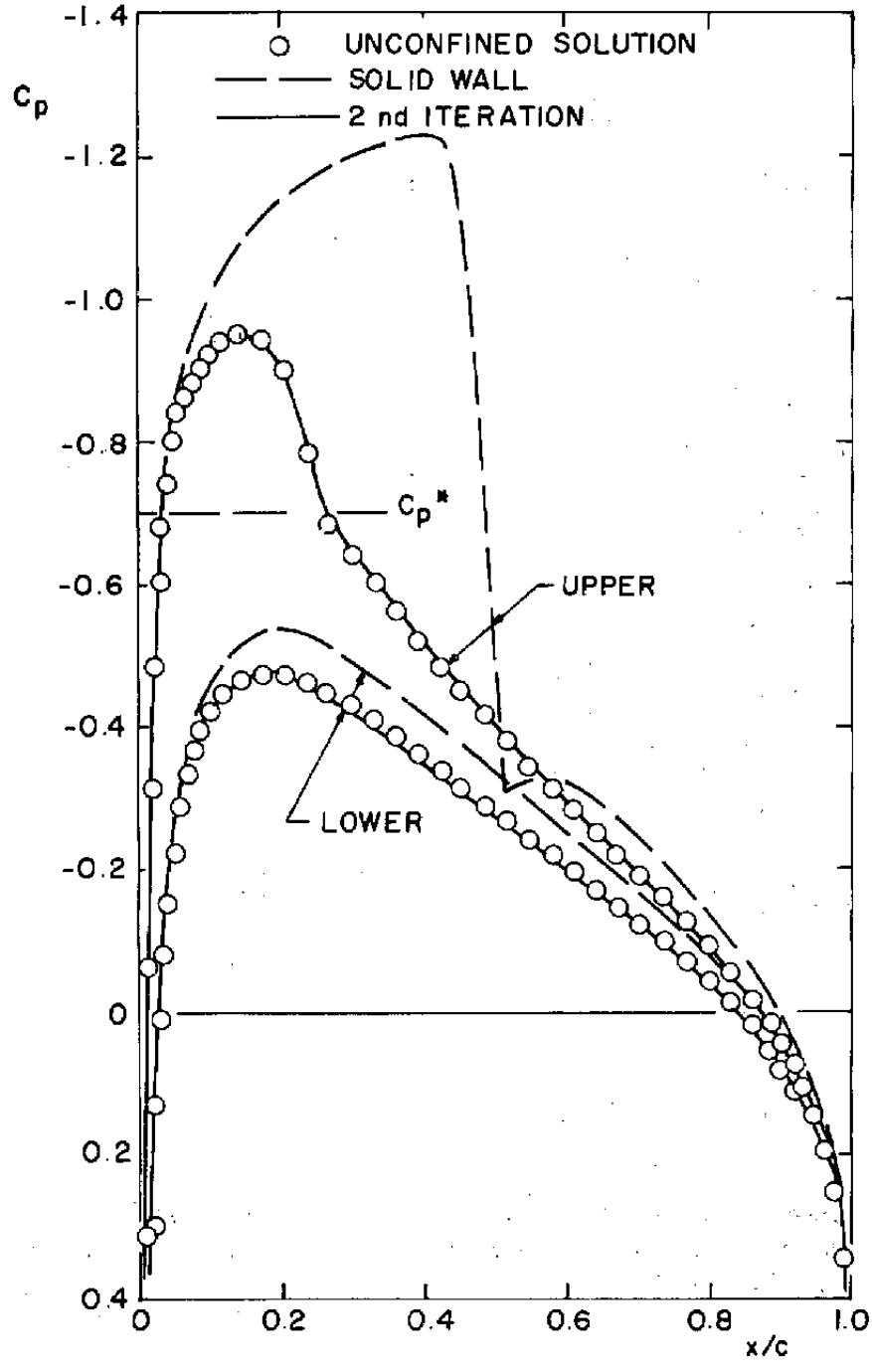

Figure 12. Airfoil surface pressure distributions based on one-step results for NACA 0012 airfoil, h/c = 1.0, M = 0.72, α = 1.0.

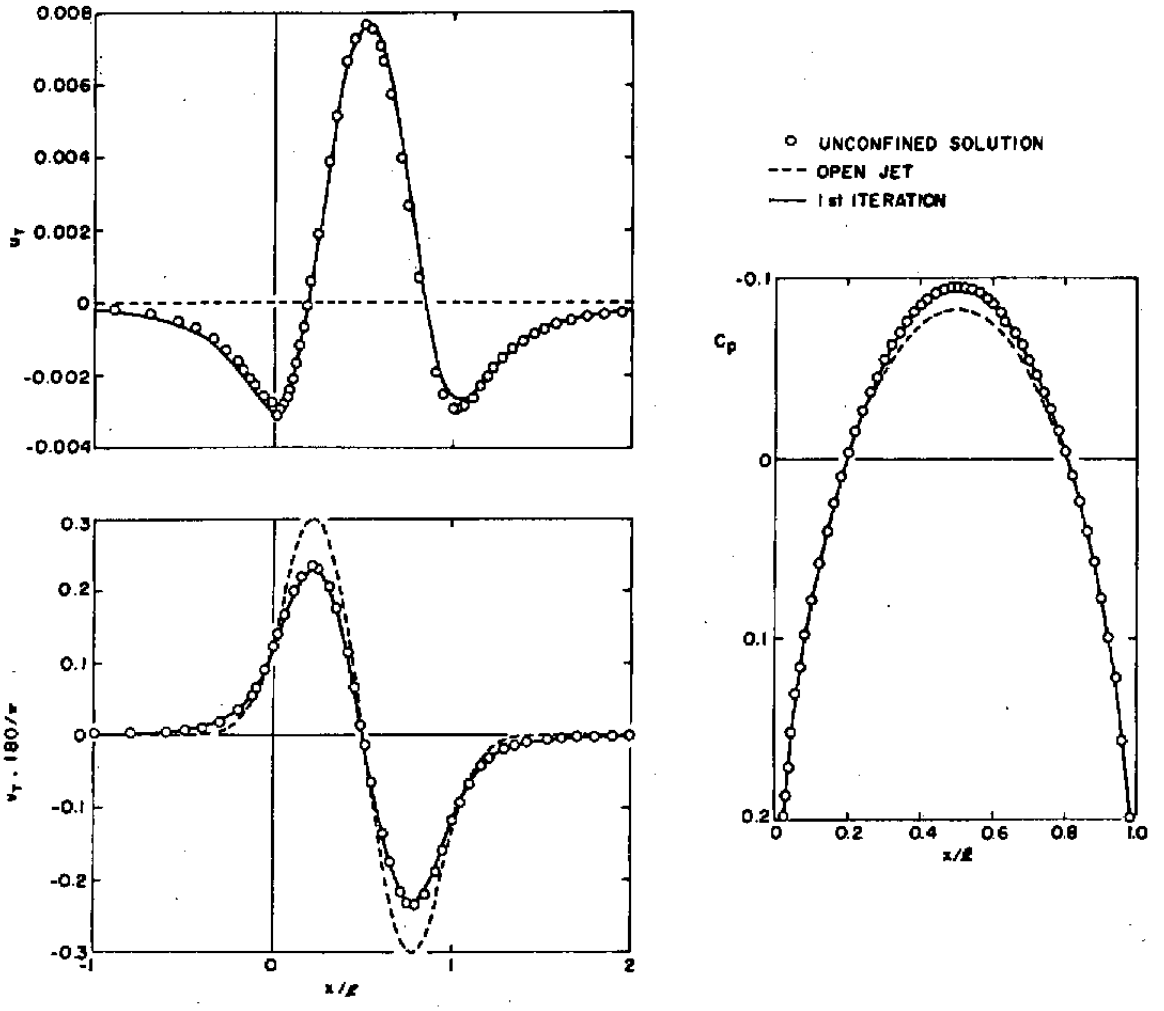

Figure 13. Distributions of velocity components at the control surface ($R/\ell = 0.5$) and body surface pressure on a parabolic arc body of revolution, $\ell/d = 10$, $M = 0.9$, $\alpha = 0$.

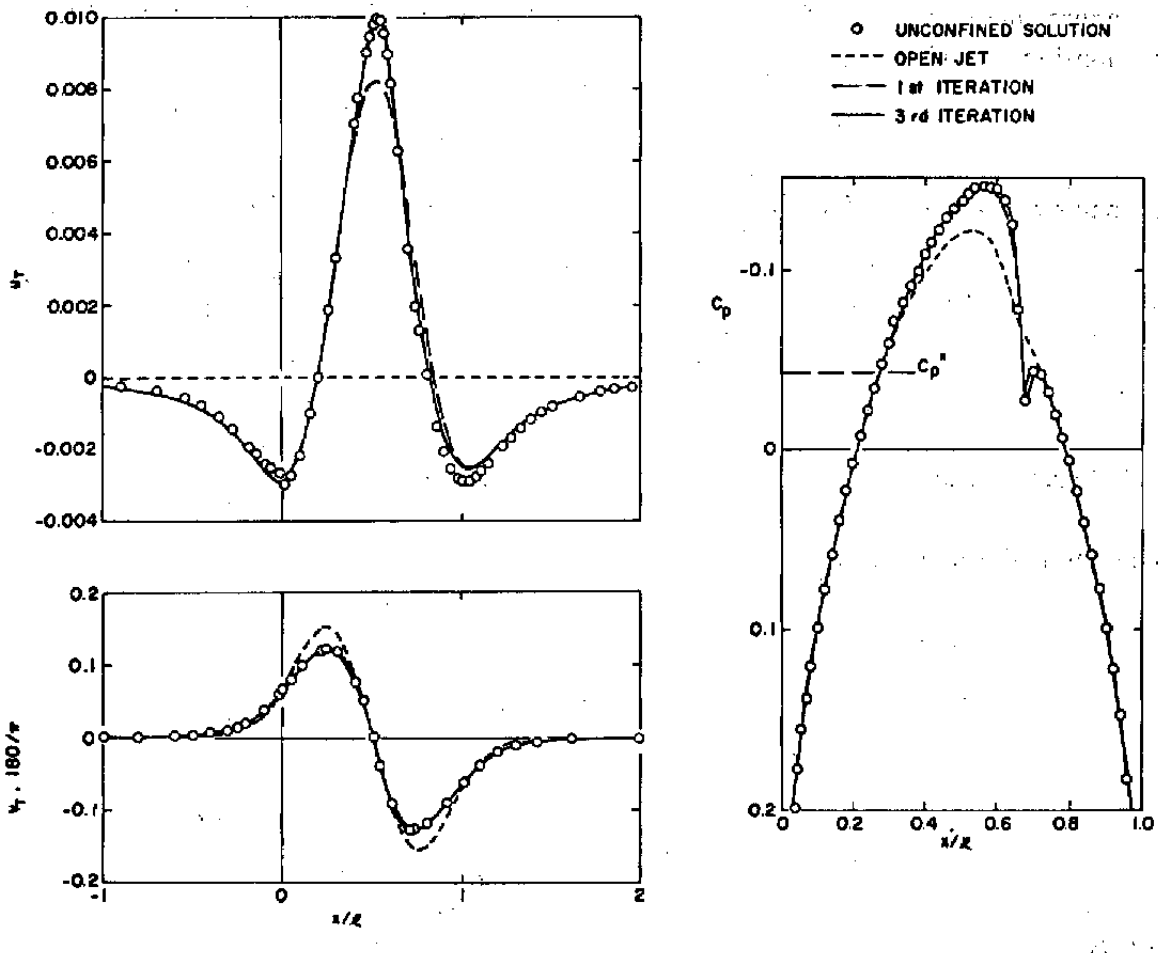

Figure 14. Distributions of velocity components at the control surface (R/ℓ = 1.0) and body surface pressure on a parabolic arc body of revolution, ℓ/d = 10, M = 0.975, α = 0.

APPENDIX A

INVERSION OF THE AXISYMMETRIC ONE-STEP CONVERGENCE FORMULAE

Unlike the case of two-dimensional flow, an analytic inversion of the one-step convergence formulae for axisymmetric flow, Eq. (45), into the physical plane is not available. An approximate inversion is derived as shown below. Using the exterior flow functional relationship, Eq. (24),

$$\bar{u}_E(p, R) = \frac{i}{\beta}\frac{p}{|p|}\frac{K_o(|p|\beta R)}{K_1(|p|\beta R)}\bar{v}_T(p, R)$$

the one-step equation in the transformal plane, Eq. (45), may be rewritten in the form

$$\bar{u}_\infty(p, R) = \frac{1}{2}\left[\bar{u}_T(p,R) + \bar{u}_E(p,R)\right] + \frac{i}{\beta}\frac{p}{|p|}\frac{K_o(\lambda)}{K_1(\lambda)}\left[\frac{1}{2} - \lambda K_o(\lambda) I_1(\lambda)\right]\bar{v}_T(p, R)$$

$$-\left[\frac{1}{2} - \lambda K_o(\lambda) I_1(\lambda)\right]\bar{u}_T(p, R)$$

(All Bessel functions I_1, K_o, K_1 have argument $\lambda = |p|\beta R$.)

This can be inverted into the physical plane as

$$u_\infty(x,R) = \frac{1}{2}\left[u_T(x,R) + u_E(x,R)\right]$$

$$-\frac{1}{\pi\beta}\sum b_m \int_{-\infty}^{\infty} \frac{(\xi - x)}{(\xi - x)^2 + (m\beta R/2)^2} v_T(\xi, R)\, d\xi$$

$$-\frac{1}{\pi}\sum c_m \int_{-\infty}^{\infty} \frac{m\beta R/2}{(\xi - x)^2 + (m\beta R/2)^2} u_T(\xi,R)\, d\xi$$

where

$$u_E(x,R) = \frac{1}{\pi\beta}\oint_{-\infty}^{\infty} \frac{v_T(\xi,R)}{\xi - x} d\xi - \frac{1}{\pi\beta}\sum a_m \int_{-\infty}^{\infty} \frac{(\xi - x)}{(\xi - x)^2 + (m\beta R/2)^2} v_T(\xi,R)\, d\xi$$

The a_m, b_m, and c_m are, respectively, the coefficients of the exponential series approximation of the following Bessel functions:

$$\frac{K_o(\lambda) - K_1(\lambda)}{K_1(\lambda)} = \sum_{m=1}^{M} a_m e^{-m\lambda/2}$$

$$\frac{K_o(\lambda)}{K_1(\lambda)}\left[\frac{1}{2}-\lambda K_o(\lambda)\, I_1(\lambda)\right] = \sum_{m=1}^{M} b_m\, e^{-m\lambda/2}$$

$$\frac{1}{2}-\lambda K_o(\lambda)\, I_1(\lambda) = \sum_{m=1}^{M} c_m\, e^{-m\lambda/2}$$

The coefficients a_m, b_m, c_m, are determined by truncating the curve fits at $M = 5$. The value of these coefficients used in the numerical demonstrations in Section 5 are as follows:

$$a_m = \{-1.748,\ 9.557,\ -26.203,\ 31.026,\ -13.624\}$$

$$b_m = \{0.661,\ -1.979,\ 13.078,\ -0.609,\ -1.137\}$$

$$c_m = \{0.835,\ -3.379,\ 8.115,\ -7.387,\ 2.323\}$$

$$m = 1, 2, \ldots, 5$$

NOMENCLATURE

a_m,b_m,c_m	Coefficients of exponential curve fits (Appendix A)
C_p	Small disturbance pressure coefficient, -2u
c	Airfoil chord
d	Maximum diameter of axisymmetric body
F	2-D model profile
G	Defined in Eq. (17) for 2-D flow and Eq. (31) for axisymmetric flow
h	Location of 2-D control surface (Fig. 2)
k	Relaxation factor in physical plane
ℓ	Axisymmetric body length
p	Fourier transform parameter
Q	Axisymmetric model profile
R	Location of axisymmetric control surface (Fig. 4)
S	Control surface
u,v	Perturbation velocity components parallel and normal to free stream, respectively (normalized by free-stream velocity)
x,r	Axisymmetric coordinates parallel and normal to free stream, respectively
x,z	2-D coordinates parallel and normal to free stream, respectively
α	Airfoil incidence, deg
β	$\sqrt{1 - M^2}$
γ	2-D model camber and incidence
Λ	Defined in Eq. (21) for 2-D flow and Eq. (35) for axisymmetric flow
ϕ	Perturbation velocity potential normalized by free-stream velocity

Ω	Defined in Eq. (20) for 2-D flow and Eq. (34) for axisymmetric flow
ω	Relaxation factor in transform plane

Subscripts

A	Asymmetric component
E	Exterior region
m	Summation index
s	Symmetric component
T	Tunnel interior region
∞	Free-air condition

Superscripts

(n)	Iteration number
*	Critical value

Notations

$\| \|$	Absolute value
$\bar{(\ )}$	Quantity in transform plane
Σ	Summation